ADVANCED ENERGY MATERIALS

Supporting Information

for *Adv. Energy Mater.*, DOI 10.1002/aenm.202301041

Elucidating the Role of Prelithiation in Si-based Anodes for Interface Stabilization

*Shuang Bai, Wurigumula Bao, Kun Qian, Bing Han, Weikang Li, Baharak Sayahpour, Bhagath Sreenarayanan, Darren H.S. Tan, So-yeon Ham and Ying Shirley Meng**

Supplemental Information

Elucidating the Role of Prelithiation in Si-based Anodes for Interface Stabilization

Shuang Bai,[1] Wurigumula Bao,[2,3] Kun Qian,[2] Bing Han,[2] Weikang Li,[2] Baharak Sayahpour,[1] Bhagath Screenarayanan,[2] Darren H.S. Tan,[2] So-yeon Ham,[1] and Ying Shirley Meng[1,2,3,*]

1. Materials Science and Engineering, University of California San Diego, La Jolla, CA 92093, United States.
2. Department of NanoEngineering, University of California San Diego, La Jolla, CA 92093, United States.
3. Pritzker School of Molecular Engineering, University of Chicago, Chicago, IL 60637, United States.

Corresponding author: shirleymeng@uchicago.edu

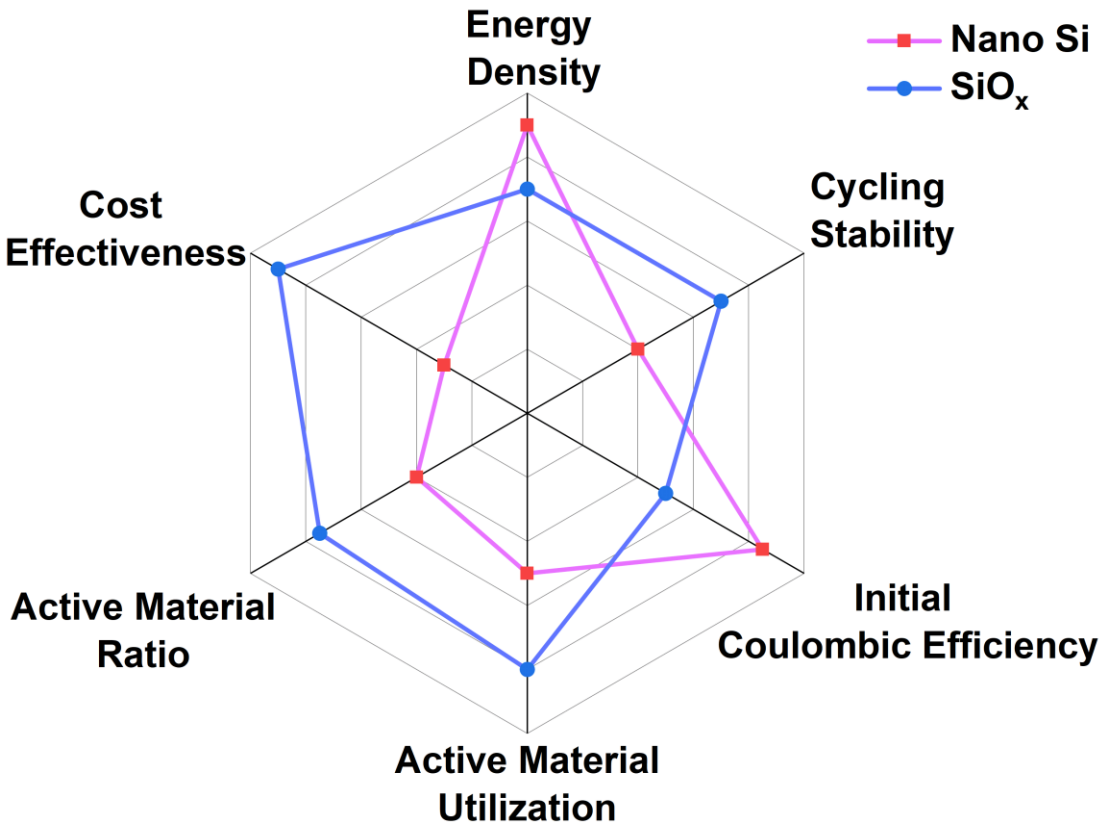

Figure S1. Performance metrics comparison of Si-based anodes.

Table S1. Literature summary of prelithiation method and its impact on ICE in half cell of SiO_x and Si.

	Anode Materials	AM ratio (%)	ICE before prelithiation (%)	ICE after prelithiation (%)	Method	Ref.
SiO_x	c-SiO	80	73.6	94.9	Half cell	[16]
	SiO	80	79.4	89.2	Short-circuit	[17]
	SiO	70	58.5	82.0	Chemical	[19]
	SiO	60	66.5	92.5	Chemical	[20]
	SiO_x@C	80	75.7	98.0	Half cell	[21]
	SiO/Gr	18	59.3	90.5	Chemical	[22]
	SiO	70	63.0	96.0	Short-circuit	This work
Si	Si/C	30	38.0	97.0	Short-circuit	[23]
	c-Si	15	80.4	89.0	Chemical	[24]
	Si@SiO	60	56.8	89.1	Chemical	[25]
	Si/Gr	21	77.2	99.6	Chemical	[26]
	Si/CNT	5	47.0	102.0	Half cell	[18]
	Si	70	89.0	101.0	Short-circuit	This work

Table S2. Literature summary of prelithiation method and its impact on ICE and capacity retention in full cell using SiO_x or Si anode.

	Anode Materials	**AM ratio (%)**	**Cathode Materials**	**ICE before prelithiation (%)**	**ICE after prelithiation (%)**	**Capacity Retention (Cycle Number)**	**Ref.**
SiO_x	c-SiO	80	NCA	58.8	85.3	61(100)	[16]
	SiO	80	NMC622	68.9	87.3	74(200)	[17]
	SiO	70	LCO	66.4	93.6	75(15)	[19]
	SiO	60	NMC622	25.0	60.0	52(100)	[20]
	SiOx@C	80	LFP	62.1	98.0	78(100)	[21]
	SiO/Gr	18	NMC622	40.0	88.0	70(800)	[22]
	SiO	70	LFP	44.0	93.9	77(200)	This work
Si	Si/C	30	NMC811	40.4	82.2	52(50)	[23]
	c-Si	15.6	LCO	76.4	92.5	80(366)	[24]
	Si@SiO	60	LFP	59.0	91.1	83(100)	[25]
	Si/Gr	21	NMC811	71.0	89.6	86(1000)	[26]
	Si/CNT	5.27	LFP	NA	91.0	NA	[18]
	Si	70	LFP	79.4	93.6	44(200)	This work

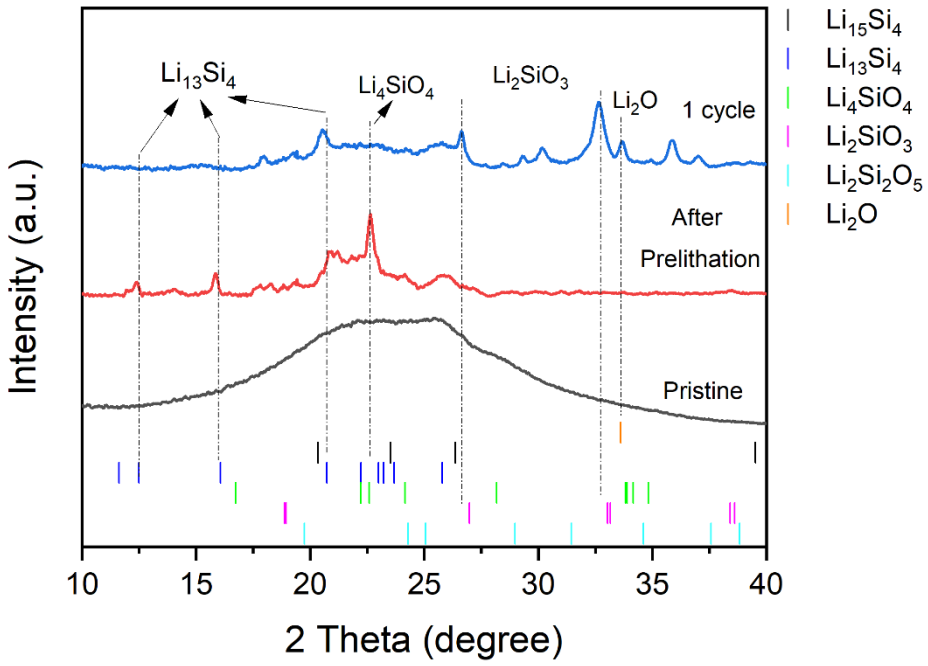

Figure S2. XRD patterns of pristine $SiO_{1.3}$, prelithiated-before cycle and prelithiated-1 cycle $SiO_{1.3}$ with standard sample diffraction peak positions.

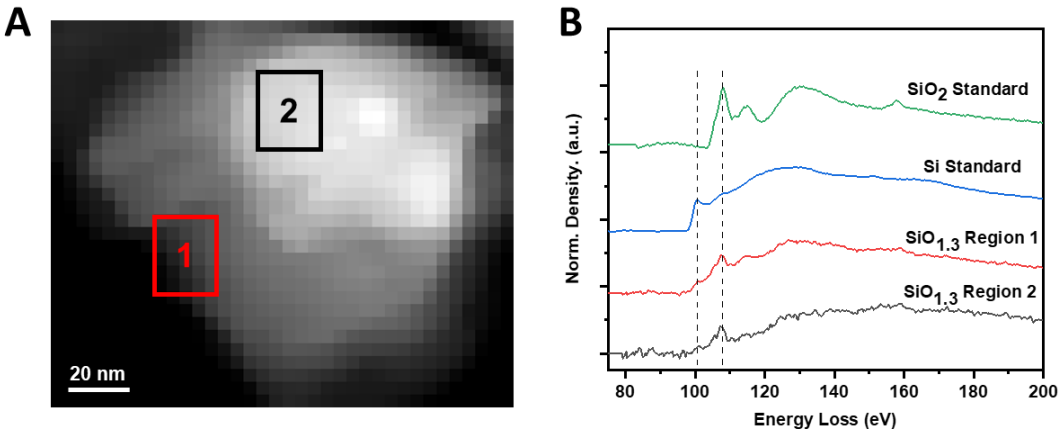

Figure S3. Microstructure information of pristine $SiO_{1.3}$ powder using STEM-EELS. (A) HAADF image of pristine $SiO_{1.3}$ powder and (B) corresponding EELS spectra of surface and bulk region together with the Si L-edge from the standard powder samples Si and SiO_2.

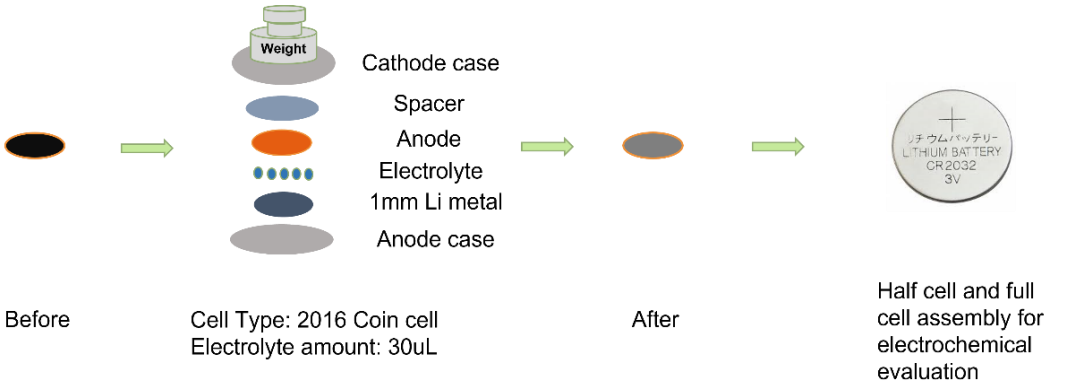

Figure S4. Schematic of prelithiation setup and process through the short-circuit electrochemical method.

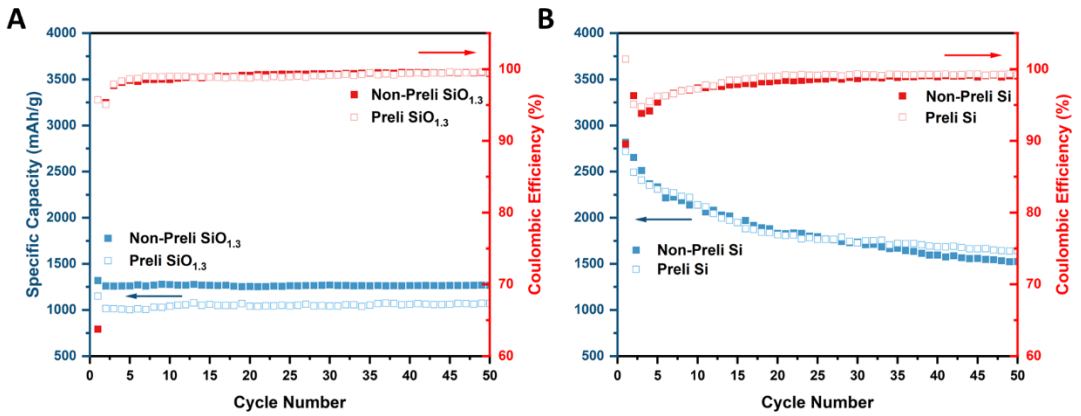

Figure S5. (A) Long-term cycling performance of prelithiated and non-prelithiated $SiO_{1.3}$ in half cell. (B) Long-term cycling performance of prelithiated and non-prelithiated μSi in half cell. The galvanostatic discharge/charge test was carried out at C/20-rate (1 C =2000 mAh/g for $SiO_{1.3}$ and 1 C=3400 mAh/g for μSi) for the initial two cycles. The cells were then charged and discharged at C/10-rate for the rest of the cycles.

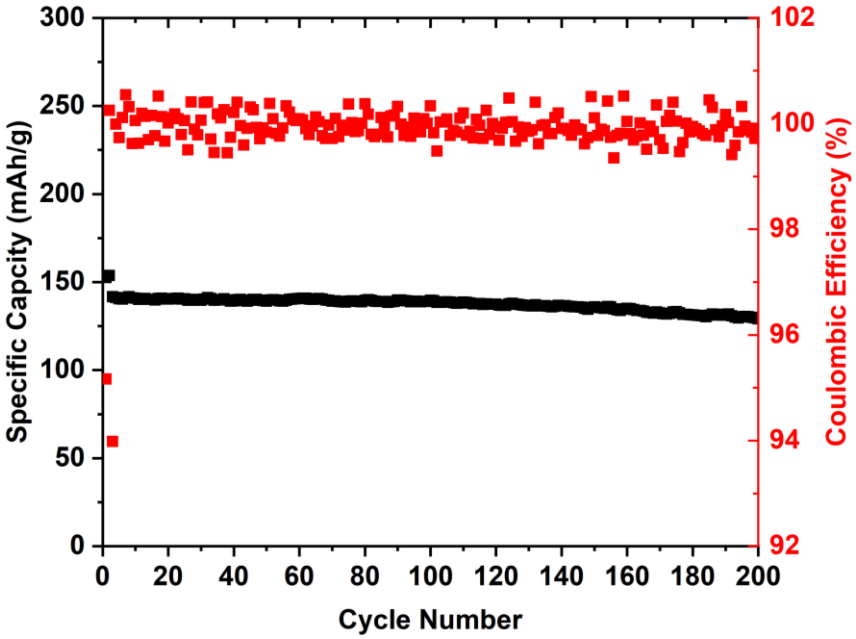

Figure S6. Long-term cycling performance of LFP cathode in half cell with Li metal as the counter electrode. (Cycling conditions: 2.6 V-3.8 V for initial two cycles at C/10 rate, then C/3 for the rest of cycles. 1 C=170 mAh/g)

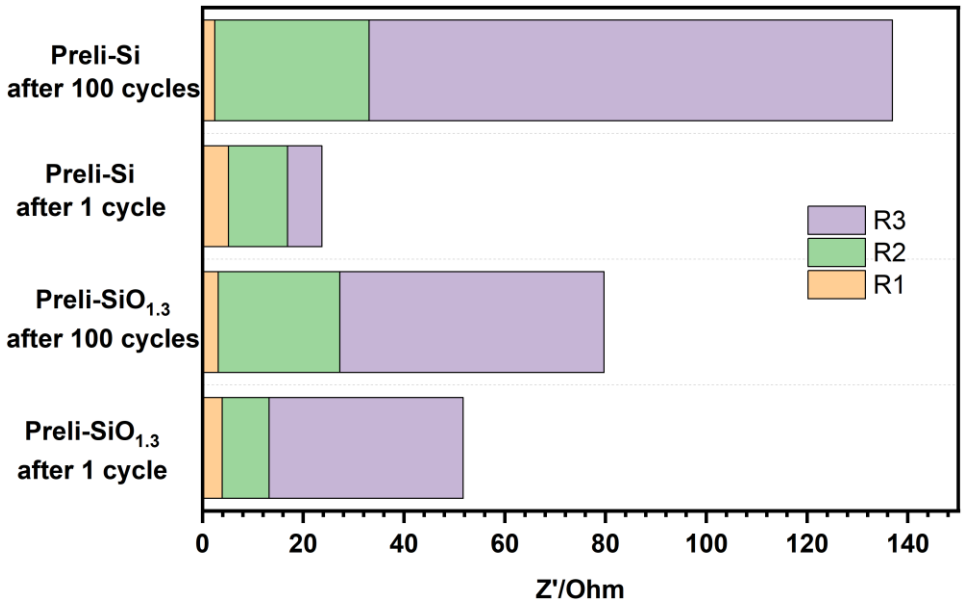

Figure S7. Resistance values of different circuit components based on the fitting results.

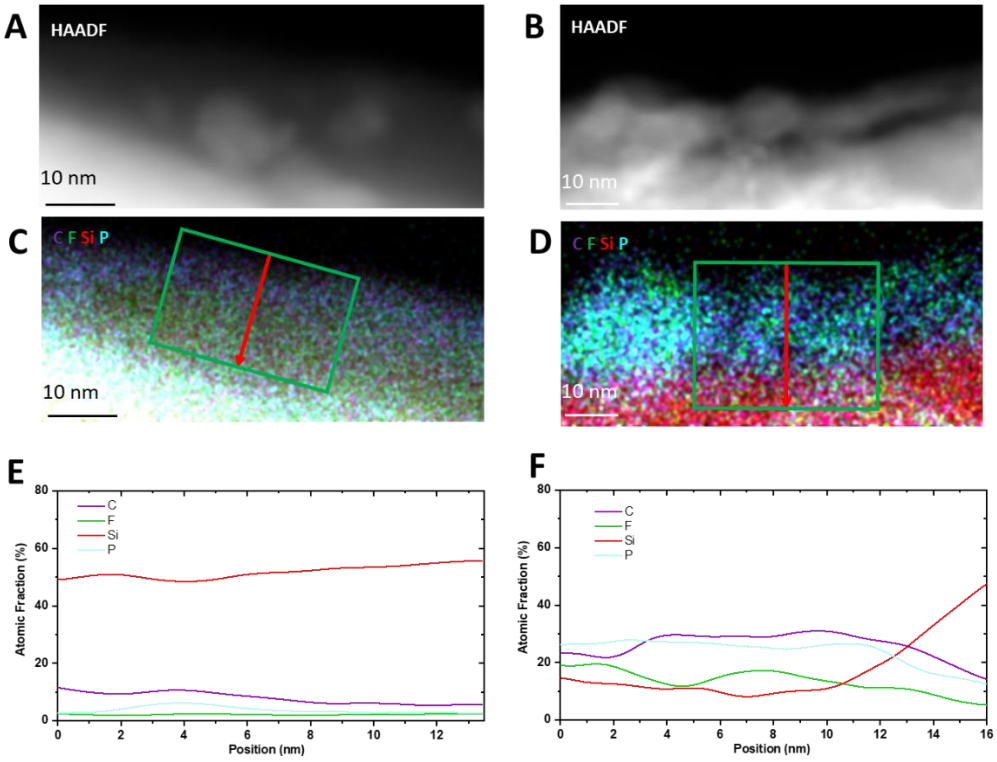

Figure S8. (A) HAADF image of prelithiated $SiO_{1.3}$ after the initial discharge and (C) its corresponding EDX mapping with (E) line scan analysis from surface to bulk. (B) HAADF image of lithiated $SiO_{1.3}$ in the half cell to the same potential after the initial discharge and (D) its corresponding EDX mapping with (F) line scan analysis from surface to bulk.

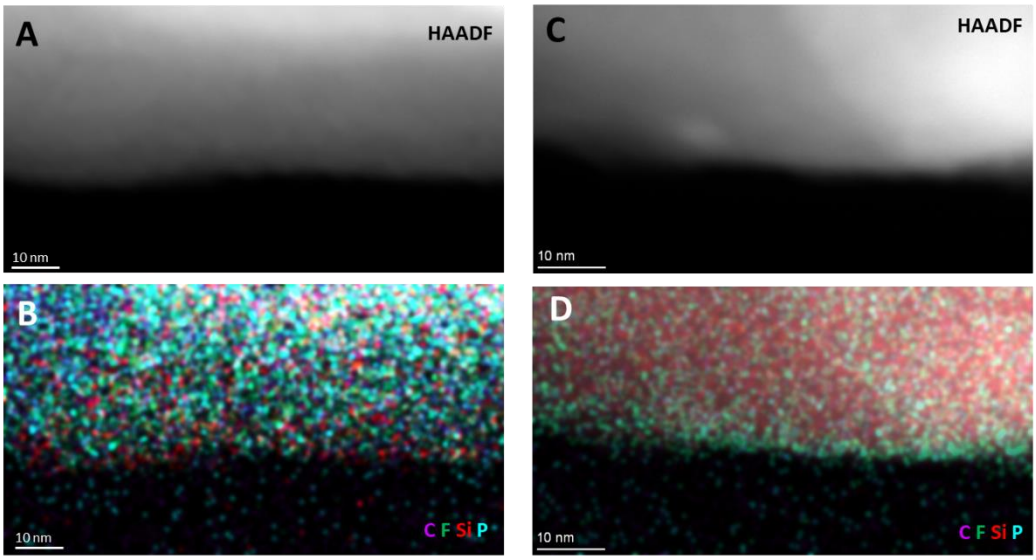

Figure S9. (A) HAADF image of prelithiated µSi using the short-circuit electrochemical method and (B) its corresponding EDX mapping. (C) HAADF image of lithiated µSi in the half cell to the same potential as the prelithiated sample and (D) its corresponding EDX mapping.

Table S3. Summary of identified SEI components and their lattice planes with corresponding d-spacing. (The significant digit of D-spacings in this table is within the resolution limit of HRTEM and the corresponding FFT for phase identification.)

COMPONENT	LATTICE PLANE	D-SPACING (Å)
LiF	(002)	2.0
	(111)	2.3
Li_2CO_3	(002)	2.8
	(20-2)	2.9
Li_2O	(111)	2.6
	(022)	1.6
	(113)	1.3
Li_4SiO_4	(114)	3.1
	(402)	2.5
	(11-3)	3.9
$Li_2Si_2O_5$	(104)	3.0
	(111)	3.5
Li_2SiO_3	(111)	3.3

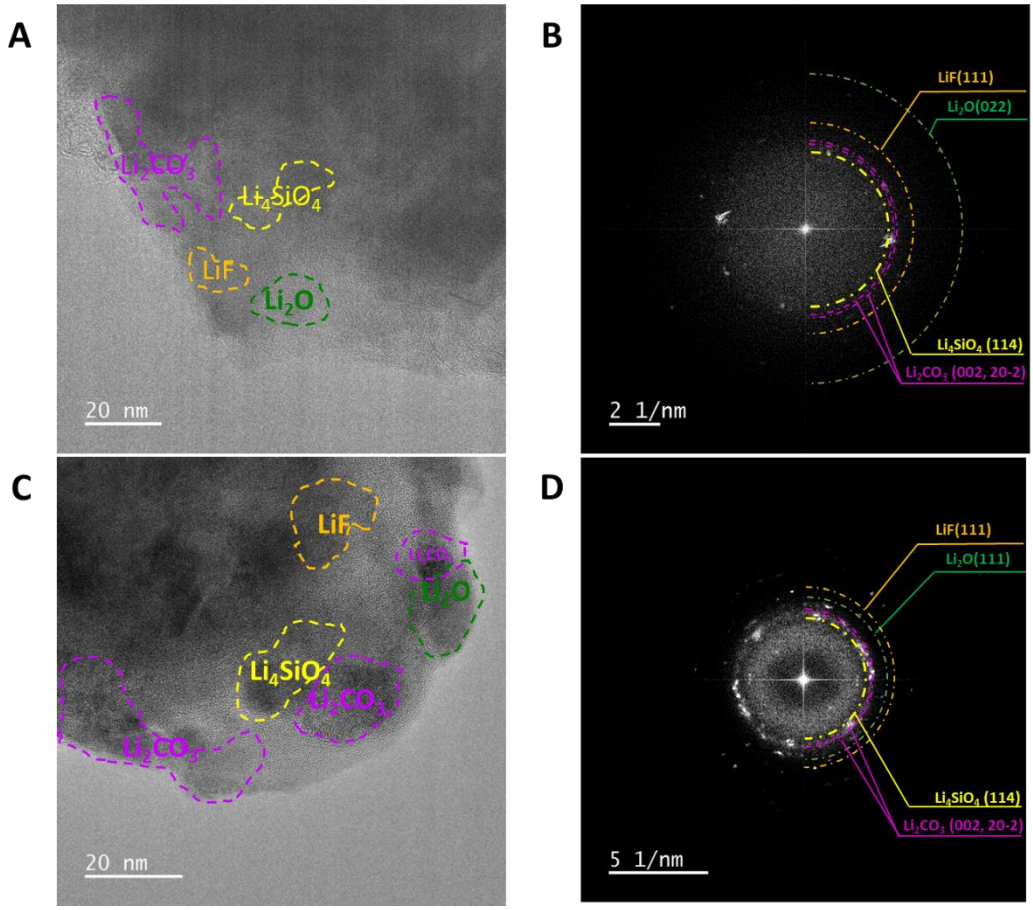

Figure S10. (A) HRTEM on one particle of lithiated $SiO_{1.3}$ in the half cell to the same potential and (B) its corresponding FFT pattern. (C) HRTEM on another particle of lithiated $SiO_{1.3}$ in the half cell to the same potential and (D) its corresponding FFT pattern.

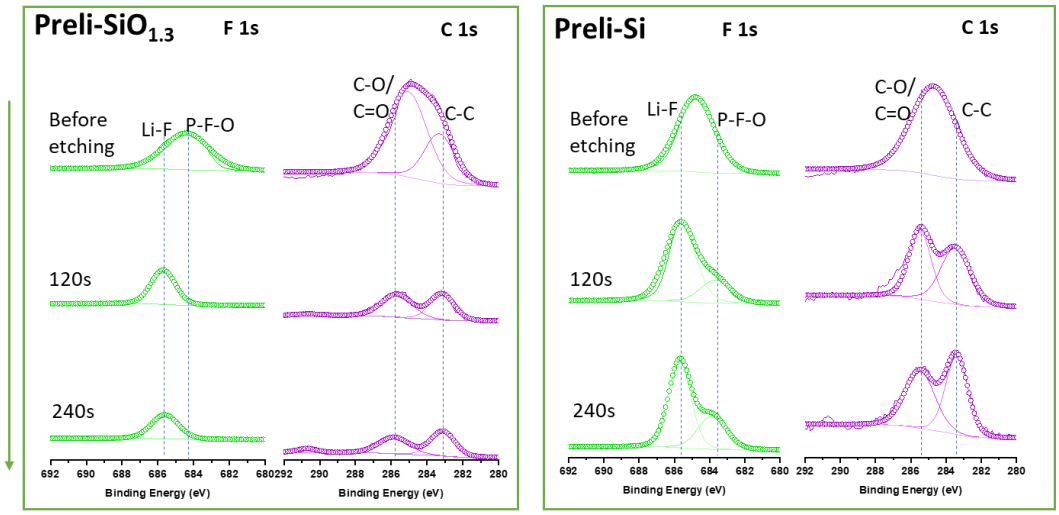

Figure S11. The XPS depth profiling of F 1s and C 1s spectra of the prelithiated $SiO_{1.3}$ and μSi anodes.

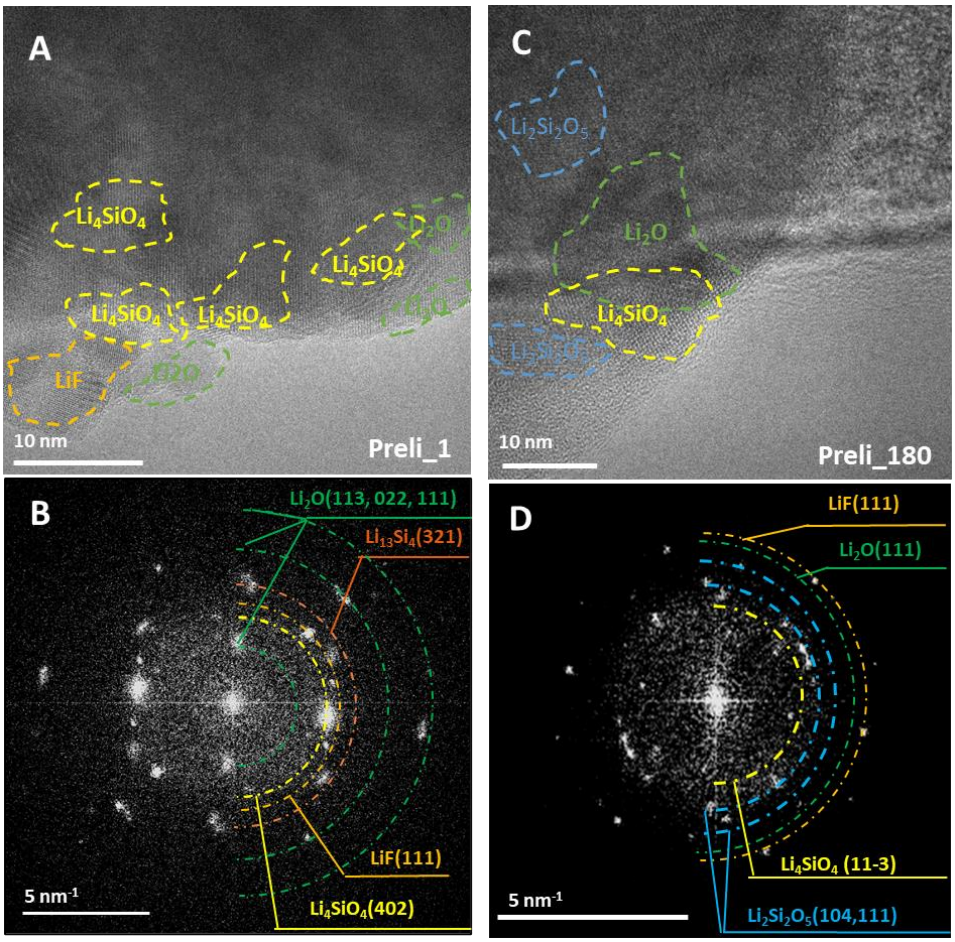

Figure S12. (A) HRTEM of prelithiated $SiO_{1.3}$ after 1 cycle and (B) its corresponding FFT pattern. (C) HRTEM of prelithiated $SiO_{1.3}$ after 180 cycles and (D) its corresponding FFT pattern.

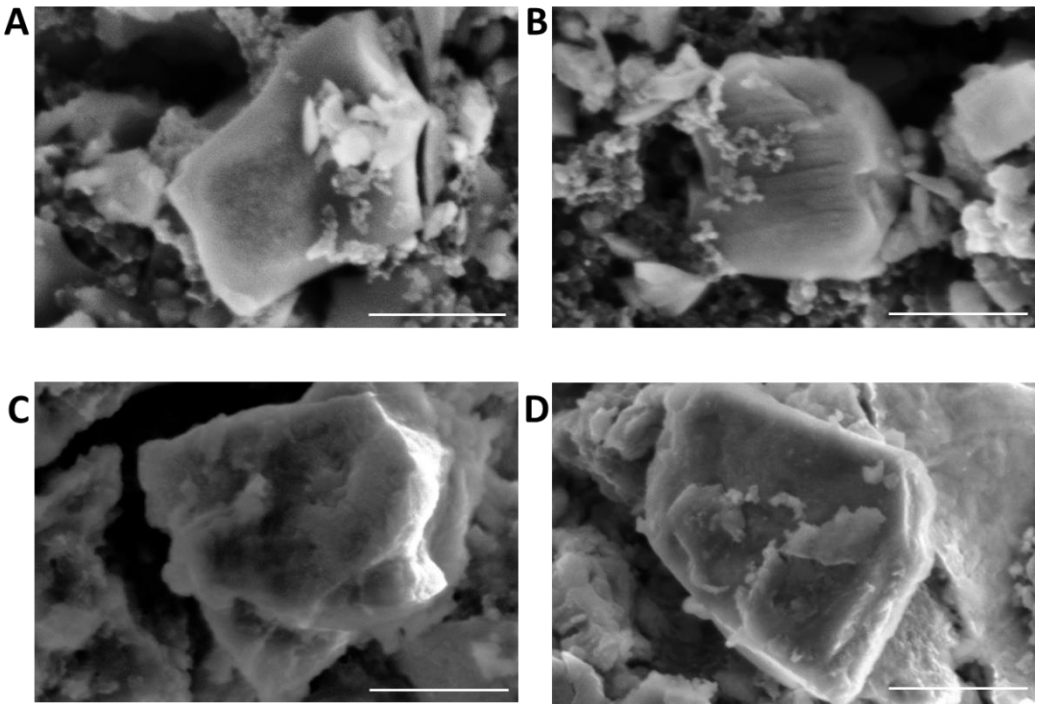

Figure S13. SEM images of pristine $SiO_{1.3}$ (A, B) and prelithiated $SiO_{1.3}$ after 100 cycles (C, D). All the scale bars in SEM images represent 1 μm.